Available online at www.sciencedirect.com
ScienceDirect
Trans. Nonferrous Met. Soc. China 34(2024) 3978−3991
Transactions of Nonferrous Metals Society of China
www.tnmsc.cn

Modulation of microstructure and properties of Cu−Ni−Sn alloy by addition of trace Ti

Ying-lin HU[1], Zi-luo CHENG[1], Xiao-na LI[1,2], Zhu-min LI[3], Yuan-di HOU[1], Min LI[1], Mian YANG[1], Yue-hong ZHENG[4], Chuang DONG[1,2]

1. School of Materials Science and Engineering, Dalian University of Technology, Dalian 116024, China;
2. Key Laboratory of Materials Modification by Laser, Ion and Electron Beams, Ministry of Education, Dalian University of Technology, Dalian 116024, China;
3. School of Materials Science and Engineering, Anhui Polytechnic University, Wuhu 241000, China;
4. State Key Laboratory of Advanced Processing and Recycling of Nonferrous Metals, Lanzhou University of Technology, Lanzhou 730050, China

Received 22 April 2023; accepted 13 October 2023

Abstract: The segregation of Sn and discontinuous precipitation at grain boundaries are detrimental to the strength, ductility, and machinability of the Cu−Ni−Sn alloy. A strategy to solve the above problems is multi-component composition design by introducing strong enthalpic interaction element. In this work, a series of $Cu_{80}Ni_{15}Sn_{5-x}Ti_x$ (at.%) alloys were designed by cluster-plus-glue-atom model, and the effects of Ti content on the microstructure and properties of the alloys were systematically investigated using TEM and other analysis methods. The results demonstrate that Ti can effectively inhibit the segregation and discontinuous precipitation while promoting continuous precipitation to improve the high-temperature stability of the alloys. As the Ti content increases, the distribution of Ti changes from uniform distribution to predominant precipitation. The hardness and conductivity of the alloy exceed those of the C72900 (Cu−15Ni−8Sn (wt.%)) commercial alloy and the $Cu_{80}Ni_{15}Sn_5$ (at.%) reference alloy when Ti is in the solution state.

Key words: Cu−Ni−Sn alloy; microstructure; properties; cluster-plus-glue-atom model; segregation; discontinuous precipitation; enthalpic interaction

1 Introduction

Cu−Ni−Sn alloys have been widely used in the electronics industry for springs, electronic connectors, bushings, and bearings owing to their high strength, elasticity, excellent resistance to stress relaxation, corrosion, and wear [1−4]. Among Cu−Ni−Sn alloys systems, Cu−15Ni−8Sn (wt.%) alloy has emerged as a new generation of the environmentally friendly conductive elastic materials, due to its comparable strength to that of typical Cu−Be alloys, as well as its simple production process, low cost, and absence of toxic gas generation during production [5−7]. However, it is difficult to avoid severe segregation of Sn during solidification, since the melting point of Sn is much lower than that of Cu and Ni. Moreover, discontinuous precipitation at grain boundaries is prone to occur during aging because the faster diffusion of Sn in Cu compared to Cu and Ni renders Sn to be easily enriched at the grain boundaries [8,9]. The aforementioned problems will degrade the homogeneity of the microstructure

Corresponding author: Xiao-na LI, Tel: +86-13664219433, E-mail: lixiaona@dlut.edu.cn
DOI: 10.1016/S1003-6326(24)66652-5

and composition, and deteriorate the strength, ductility, and machinability of the alloy, thus reducing the production yield of the thin strip.

Rapid solidification techniques upgrade the cooling rate of the alloy during solidification, partially suppressing the Sn segregation and discontinuous precipitation. However, achieving a uniform distribution of Sn through long-range diffusion has not yet been accomplished [10−13]. Moreover, the above techniques are faced with various challenges, such as a complex process, high costs, and numerous metallurgical defects. Therefore, the aforementioned problems cannot be solved solely within the Cu−Ni−Sn ternary alloy system and need to be approached through multi-component composition design [14−17]. Previous studies [18−20] have found that the addition of elements that can form compounds with Ni, such as Nb, V, and Si, effectively optimizing the microstructure and improving the performance of Cu−Ni−Sn alloys. Nano-sized Ni_2Si, Ni_3Si, Ni_3Nb, or Ni_3V phases precipitated in the matrix can delay the peak age-hardening process while still maintaining the strengthening effect. The $Ni_{31}Si_{12}$ or Ni_3Nb phases, which precipitate at the grain boundaries, can occupy the nucleation sites of the discontinuous precipitation, thereby inhibiting it.

In the Cu−Ni−Sn system, the Cu matrix and the $D0_{22}$ or $L1_2$-γ' phase (Ni_3Sn phase, as the main strengthening phases) are multi-component systems, in which a small amount of Ni and Sn are dissolved in the Cu matrix, while a portion of Cu is dissolved in the precipitated phases [21]. The mixing enthalpies between Cu, Ni, and Sn are as follows: ΔH_{Ni-Cu}= 4 kJ/mol, ΔH_{Sn-Cu}=7 kJ/mol, and ΔH_{Ni-Sn}= −4 kJ/mol, respectively [22]. The addition of Ti, which exhibits stronger enthalpic interaction with Ni and Sn compared to Cu (ΔH_{Ni-Ti}=−35 kJ/mol, ΔH_{Sn-Ti}=−21 kJ/mol, and ΔH_{Cu-Ti}=−9 kJ/mol), is considered to reduce the solid solution of Ni and Sn in the Cu matrix and enhance the stability of the alloy, thereby inhibiting discontinuous precipitation. Meanwhile, Ti can form Cu_4Ti and $L1_2$-Ni_3Ti phases with Cu and Ni, as nano-precipitated phases that are coherent with the Cu matrix [23,24]. Therefore, the addition of Ti is expected to promote the precipitation of solutes within the matrix, thereby increasing the effect of precipitation strengthening.

In the existing studies of Cu−Ni−Sn−Ti alloys, it has been confirmed that Ti has the effect of grain refinement [25−27]. Additionally, the precipitation of the Ni_3Ti phase at grain boundaries is beneficial to suppressing the discontinuous precipitation. By adding 0.3 wt.% Ti to Cu−15Ni−8Sn (wt.%), the tensile strength and elongation of the alloy increased from 935 to 1024 MPa and from 2.7% to 17.9%, respectively [26]. Continuing to increase the Ti content, the Ni_3Ti phase became coarse and severely deteriorated the mechanical properties of the alloy. In summary, current researches on Cu−Ni−Sn−Ti alloys have mainly focused on their mechanical properties, deformation behavior, and processing techniques. However, the distribution of Ti has not been systematically studied, and there is a lack of research on the regularity of the microstructure and properties of the alloys with varying Ti content. In addition, the existing Cu−Ni−Sn−Ti alloys are mainly designed by directly adding Ti to the commercial alloys, such as C72900 (Cu−15Ni−8Sn (wt.%)). While the amount of Ti added is mostly determined through experimental exploration, there is a lack of systematic theoretical guidance.

In our previous studies [19,28], the cluster-plus-glue-atom model was introduced into the composition design of the Cu−Ni−Sn alloy. The cluster formula of alloy can be expressed as [matrix cluster formula]$_x$ [precipitate cluster formula]$_1$, and the composition can be controlled by changing x. The composition of C72900 (Cu−15Ni−8Sn (wt.%)) commercial alloy was taken as a reference, and a ternary alloy was designed using the cluster formula of $\{[Cu-Cu_{12}]Cu_3\}_4\{[Sn-Ni_{12}]Sn_3\}$ with a composition of Cu−13.43Ni−9.05Sn (wt.%) and $Cu_{80}Ni_{15}Sn_5$ (at.%). Based on this formula, a series of $Cu_{80}Ni_{15}Sn_{5-x}M_x$ (at.%, M=Si, Zn or Co) alloys with excellent comprehensive performance were designed by replacing Sn in the principal cluster with different amounts of M. In this study, a series of Cu−Ni−Sn−Ti alloys were designed by the cluster-plus-glue-atom model as above. The existential state of Ti, and the effect on stability, hardness and conductivity of Cu−Ni−Sn alloys with varying Ti content were systematically studied. Besides, the Ni−Ti compounds were promptly precipitated through the modulated heat treatment process, and their impact on the overall performance of Cu−Ni−Sn−Ti alloys was investigated.

2 Experimental

Table 1 shows the compositions of Cu−Ni−Sn−Ti alloys designed by the cluster-plus-glue-atom model. All as-cast alloys were fabricated using high-purity metal materials (99.99 Cu, 99.999 Ni, 99.99 Sn, 99.99 Ti, in wt.%) in an intermediate frequency vacuum induction furnace (NEV-SM04, Osaka, Japan) with a protective atmosphere of high-purity argon. The ingots were machined by wire cutting to the dimensions of *d*22 mm × 7 mm. The ingots were treated by homogenizing at 850 °C for 10 h before cooling in a furnace, solid solution treatment at 850 °C for 1 h followed by water quenching, then aging at 400 °C or 450 °C for 5 h before cooling in a furnace.

The morphology of alloys was observed using an optical microscope (OM, Olympus BX51, Kyoto, Japan) and a scanning electron microscope (SEM, Zeiss Supra 55, Baden-Wurttemberg, Germany). The microstructures were analyzed using X-ray diffraction (XRD, BRUKER D8 FORCUS, Karlsruhe, Germany; Cu K_α: λ=0.15406 nm, scanning speed: 4 (°)/min) and a transmission electron microscope (TEM, JEM−2100F, 200 kV, Tokyo, Japan). In situ composition analysis was performed with an electron probe microanalysis (EPMA, EPMA−1600, SHIMADZU).

The microhardness tests were conducted using a microhardness tester (HVS−1000, Beijing, China) with a load of 200 g and a loading time of 10 s. The room temperature (RT) conductivity was measured by an eddy current conductivity meter (Sigma 2008B, Xiamen, China). The variation of the molar volume fraction of precipitated phases with temperature was calculated for the $Cu_{80}Ni_{15}Sn_5$ and Cu_{80}−$Ti_{0.1875}$ alloys under equilibrium conditions using Thermo-calc software.

3 Results

3.1 Microstructure and composition

The metallurgical structures of the as-cast $Cu_{80}Ni_{15}Sn_{5-x}Ti_x$ (x=0, 0.1875, 0.625, 1.25, 1.875, and 2.5 at.%) alloys are shown in Fig. 1. The as-cast $Cu_{80}Ni_{15}Sn_5$ reference alloy (Figs. 1(a_0−a_2)) is composed of dendritic α phase, interdendritic bone-like γ phase, and lamellar α+γ phase (discontinuous precipitation, indicated by the black area in the metallurgical structures). According to the fact that the melting point of Sn is much lower than that of Cu and Ni, the γ phase and discontinuous precipitation that solidified later are regions rich in Sn. The substantial black area that appeared shows obvious compositional inhomogeneity in the reference alloy.

After adding Ti, the size of the dendrites is refined, and the discontinuous precipitation in the as-cast alloys is remarkably reduced, as depicted in Figs. 1(b_0−f_0). Apparently, Ti has a refining effect on the dendrites and effectively inhibits discontinuous precipitation and segregation.

With the increase of Ti content x, the discontinuous precipitation (black area) gradually decreases. When x is 1.25 at.%, the discontinuous precipitation is completely suppressed, the rod-like phase (~1 μm in width, as indicated by the yellow arrows in Fig. 1(d_1)) and the needle-like phase (~200 nm in width, as indicated by the red arrows in Fig. 1(d_2)) are observed. When increasing x to 1.875 at.%, the size of rod-like phase increases to ~2 μm, and its volume fraction also increases (Fig. 1(e_1)). In addition, large dark gray regions appear in dendrites (Fig. 1(e_1)). The corresponding local magnification image is shown in Fig. 1(e_2), which consists of intersecting needle-like phase (~200 nm in width, as indicated by the red arrows),

Table 1 Compositions of Cu−Ni−Sn−Ti alloys designed by cluster-plus-glue-atom model

No.	Cluster formula	Alloy composition/at.%	Designation of alloy
1	$\{[Cu-Cu_{12}]Cu_3\}_4\{[Sn-Ni_{12}]Sn_3\}$	$Cu_{80}Ni_{15}Sn_5$	$Cu_{80}Ni_{15}Sn_5$
2	$\{[Cu-Cu_{12}]Cu_3\}_4\{[Sn_{0.85}Ti_{0.15}-Ni_{12}]Sn_3\}$	$Cu_{80}Ni_{15}Sn_{4.8125}Ti_{0.1875}$	Cu_{80}−$Ti_{0.1875}$
3	$\{[Cu-Cu_{12}]Cu_3\}_4\{[Sn_{0.5}Ti_{0.5}-Ni_{12}]Sn_3\}$	$Cu_{80}Ni_{15}Sn_{4.375}Ti_{0.625}$	Cu_{80}−$Ti_{0.625}$
4	$\{[Cu-Cu_{12}]Cu_3\}_4\{[Ti-Ni_{12}]Sn_3\}$	$Cu_{80}Ni_{15}Sn_{3.75}Ti_{1.25}$	Cu_{80}−$Ti_{1.25}$
5	$\{[Cu-Cu_{12}]Cu_3\}_4\{[Ti-Ni_{12}]Sn_{2.5}Ti_{0.5}\}$	$Cu_{80}Ni_{15}Sn_{3.125}Ti_{1.875}$	Cu_{80}−$Ti_{1.875}$
6	$\{[Cu-Cu_{12}]Cu_3\}_4\{[Ti-Ni_{12}]Sn_2Ti\}$	$Cu_{80}Ni_{15}Sn_{2.5}Ti_{2.5}$	Cu_{80}−$Ti_{2.5}$

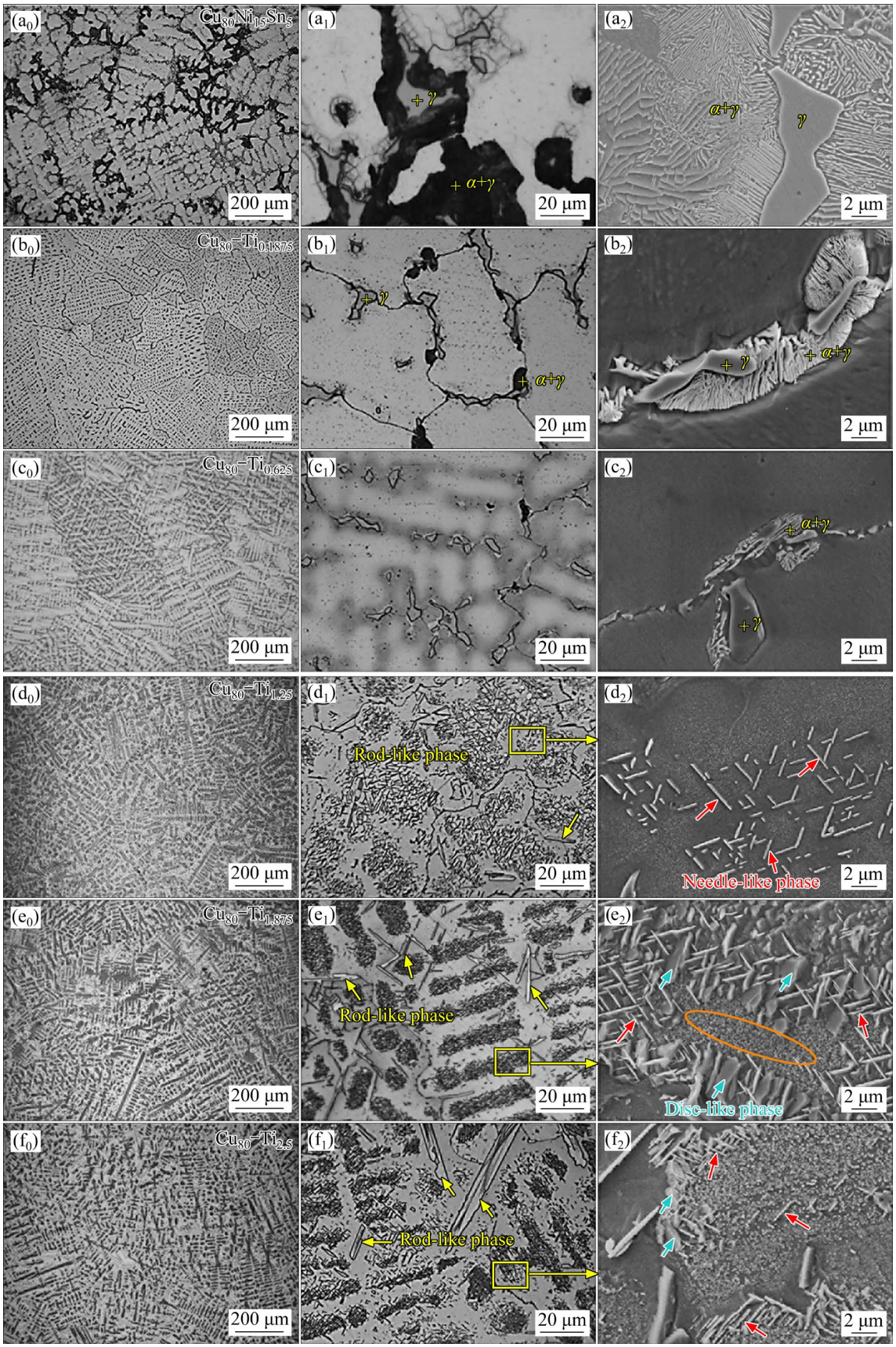

Fig. 1 Metallurgical structures for as-cast $Cu_{80}Ni_{15}Sn_{5-x}Ti_x$ alloys: (a_0−a_2) x=0; (b_0−b_2) x=0.1875 at.%; (c_0−c_2) x=0.625 at.%; (d_0−d_2) x=1.25 at.%; (e_0−e_2) x=1.875 at.%; (f_0−f_2) x=2.5 at.%

disc-like phase (~1 μm, as indicated by the cyan arrows) and the nano-precipitated phase of ~85 nm in the region (indicated by the orange oval circle) surrounded by the disc-like phases and needle-like phases. Further increasing x to 2.5 at.%, the size of rod-like phase continues to increase to ~6 μm, and the volume fraction of the needle and disc-like phase decreases, as presented in Figs. 1(f_1, f_2).

In order to further explore the distribution of Ti in the alloys, the as-cast $Cu_{80}Ni_{15}Sn_{5-x}Ti_x$ (x=0.1875, 0.625, and 2.5 at.%) alloys were selected for mapping compositional analysis by EPMA, as shown in Fig. 2. It is confirmed that the dendrites in the alloys are Cu-rich, and the inter-dendritic bone-like γ phase is rich in Ni and Sn with a wider Sn-rich region around. When x is 0.1875 at.%, Ti is uniformly distributed in the alloy, except for individual Ti-rich regions with a size of ~1 μm, as indicated by the circles in Fig. 2(a_4). When x is 0.625 at.%, the Ti-rich regions with a larger

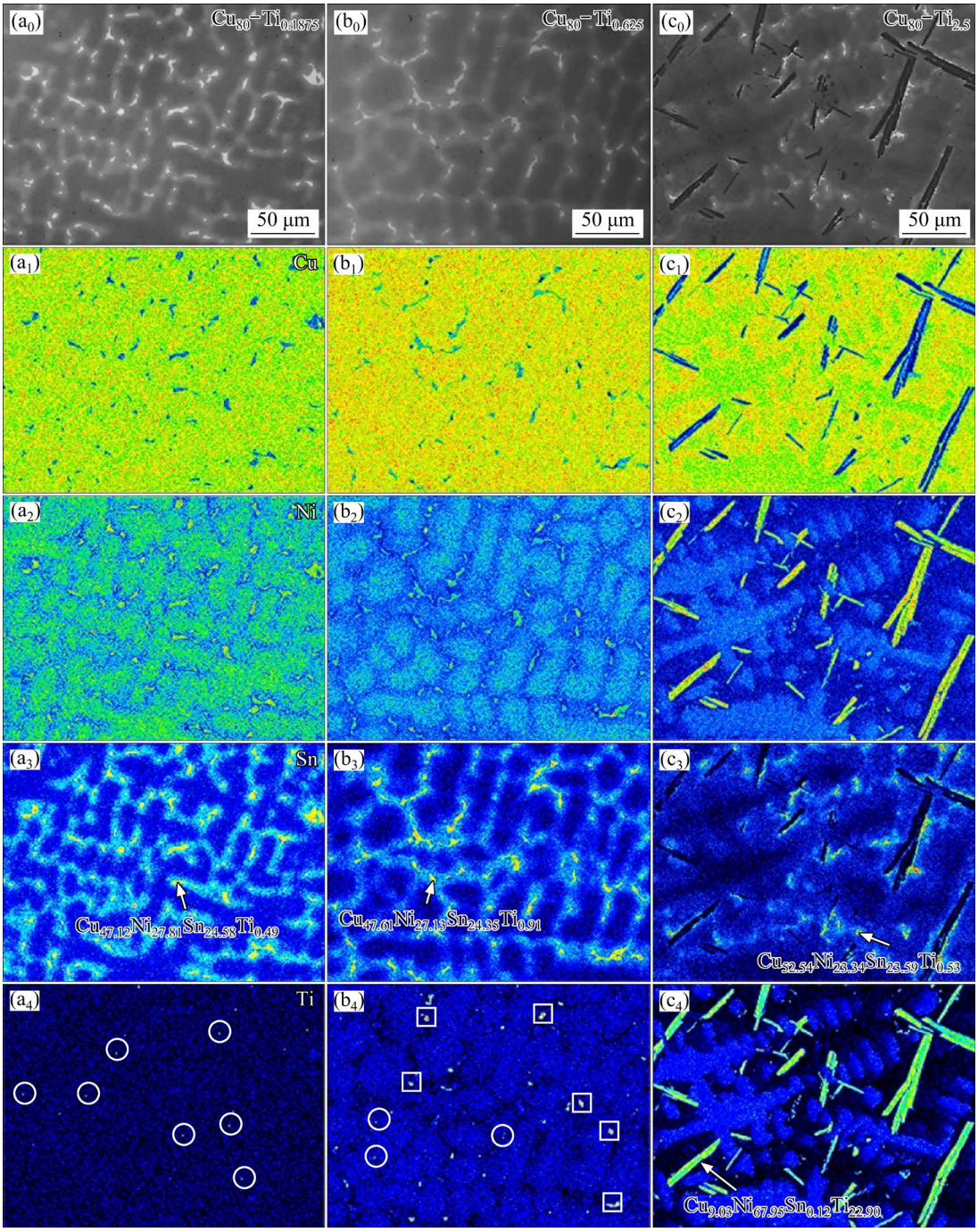

Fig. 2 Backscattered electron images and corresponding element distribution of as-cast $Cu_{80}Ni_{15}Sn_{5-x}Ti_x$ alloys: (a_0−a_4) x=0.1875 at.%; (b_0−b_4) x=0.625 at.%; (c_0−c_4) x=2.5 at.%

size of ~3 μm are observed in the dendrites (indicated by the boxes in Fig. 2(b_4)), and the volume fraction of the γ phase is reduced. After increasing x to 2.5 at.%, the volume fraction of the γ phase and the area of the surrounding Sn-rich regions is significantly decreased. However, a large number of nano-sized Ti-rich regions exist in the dendrites, and coarse rod-like phases appear in the alloy. The point composition of the rod-like phase is $Cu_{9.03}Ni_{67.96}Sn_{0.12}Ti_{22.90}$ (at.%) (Fig. 2(c_4)), which is close to $(Ni,Cu)_3Ti$. In addition, the point compositions of the γ phase in the $Cu_{80}Ni_{15}Sn_{5-x}Ti_x$ (x=0.1875, 0.625, and 2.5 at.%) alloys are $Cu_{47.12}Ni_{27.81}Sn_{24.58}Ti_{0.49}$, $Cu_{47.61}Ni_{27.13}Sn_{24.35}Ti_{0.91}$, and $Cu_{52.54}Ni_{23.34}Sn_{23.59}Ti_{0.52}$ (at.%), respectively, which are all close to $(Cu,Ni)_3Sn$ and contain trace Ti. The micro-structure of the alloy was further analyzed by TEM.

3.2 TEM images

The as-cast Cu_{80}−$Ti_{1.875}$ alloy was chosen as a representative sample for a comprehensive phase analysis. Based on the SEM images presented in Figs. 3(a, b), the alloy was divided into six distinct regions, designated as Regions 1−6.

Region 1: A rod-like phase of ~1.5 μm in width, which is confirmed as $D0_{24}$-Ni_3Ti phase according to the TEM bright field (BF) image and the corresponding selected area electron diffraction (SAED) pattern (Fig. 3(c)). The orientation relationship between the $D0_{24}$-Ni_3Ti phase and the Cu matrix is $[11\bar{2}0]_{D0_{24}\text{-}Ni_3Ti}$ //$[110]_{Cu}$ and $(0001)_{D0_{24}\text{-}Ni_3Ti}$ //$(1\bar{1}\bar{1})_{Cu}$.

Region 2: Cu matrix and spherical precipitated phases of ~25 nm, the latter are identified as $L1_2$-$(Ni,Cu)_3Sn$ and $D0_{22}$-$(Ni,Cu)_3Sn$ phases according to the BF image (Fig. 3(d)), HRTEM image and the corresponding FFT patterns of the spherical phases (Fig. 3(e)). The orientation relationship between the $L1_2$-$(Ni,Cu)_3Sn$ and the Cu matrix is $[110]_{L1_2\text{-}(Ni,Cu)_3Sn}$// $[110]_{Cu}$ and $(001)_{L1_2\text{-}(Ni,Cu)_3Sn}$//$(00\bar{2})_{Cu}$. The orientation relationship between $D0_{22}$-$(Ni,Cu)_3Sn$ phase and the Cu matrix is $[110]_{D0_{22}\text{-}(Ni,Cu)_3Sn}$//$[110]_{Cu}$ and $(0\bar{1}1)_{D0_{22}\text{-}(Ni,Cu)_3Sn}$//$(1\bar{1}\bar{1})_{Cu}$.

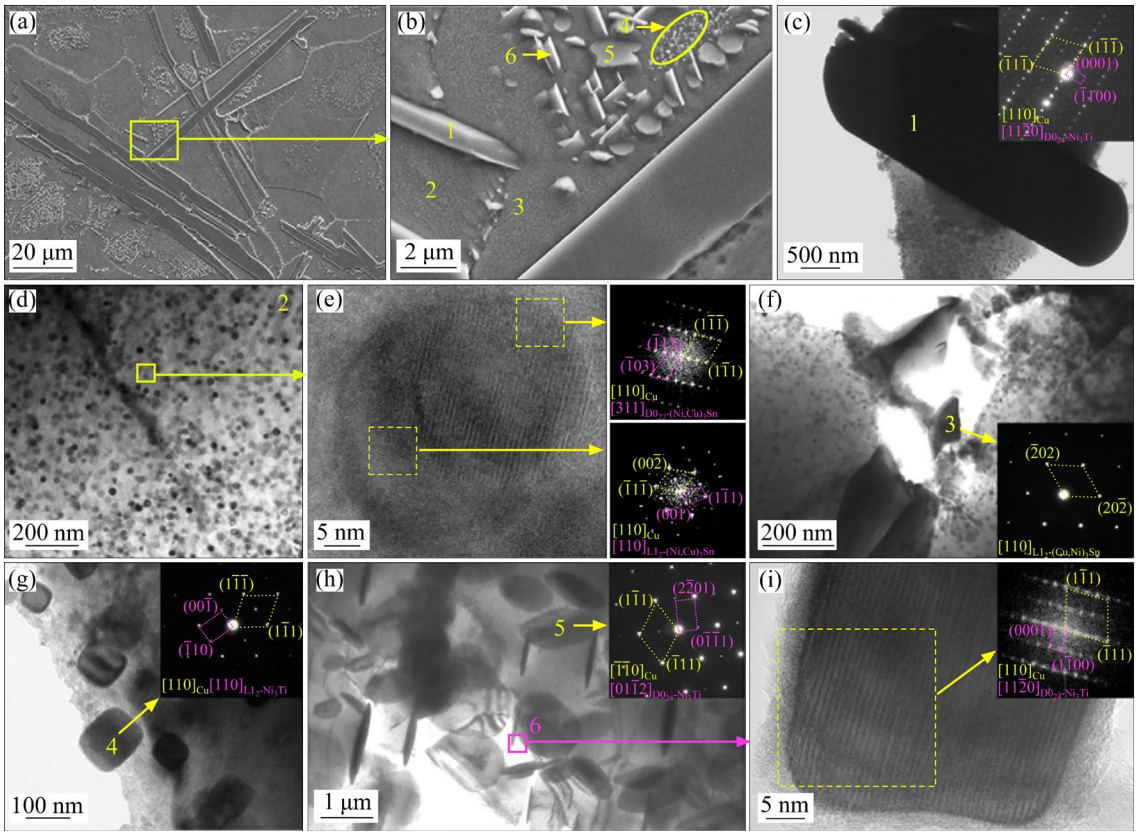

Fig. 3 Microstructures of as-cast Cu_{80}−$Ti_{1.875}$ alloy: (a, b) SEM images; (c) BF image and SAED pattern of rod-like phase; (d, e) BF image, HRTEM image and corresponding FFT patterns of intragranular continuous precipitated phases; (f) BF image and SAED pattern of nano-phases at grain boundary; (g) BF image and SAED pattern of cuboidal precipitated phase; (h) BF image and SAED pattern of disc-like precipitated phase; (i) HRTEM image and corresponding FFT pattern of needle-like phase

Region 3: γ phase at grain boundary, which is identified as $D0_3$-$(Cu,Ni)_3Sn$ phase according to the BF image and the corresponding SAED pattern (Fig. 3(f)).

Region 4: Cu matrix and cuboidal precipitated phases of ~85 nm, the latter is confirmed as the $L1_2$-Ni_3Ti phase, which is completely coherent with the Cu matrix according to the BF image and the corresponding SAED pattern (Fig. 3(g)). The orientation relationship between the $L1_2$-Ni_3Ti phase and the Cu matrix is $[110]_{L1_2\text{-}Ni_3Ti}//[110]_{Cu}$ and $(\bar{1}10)_{L1_2\text{-}Ni_3Ti}//(1\bar{1}\bar{1})_{Cu}$.

Region 5: A disc-like phase of ~1 μm, which is identified as the $D0_{24}$-Ni_3Ti phase according to the BF image and the corresponding SAED pattern (Fig. 3(h)). The orientation relationship between the disc-like $D0_{24}$-Ni_3Ti phase and the Cu matrix is: $[01\bar{1}2]_{D0_{24}\text{-}Ni_3Ti}//[\bar{1}\bar{1}0]_{Cu}$ and $(2\bar{2}01)_{D0_{24}\text{-}Ni_3Ti}//(1\bar{1}\bar{1})_{Cu}$.

Region 6: A needle-like phase of ~200 nm in width (Fig. 3(h)), which is also identified as the $D0_{24}$-Ni_3Ti phase based on the HRTEM image and the corresponding FFT pattern (Fig. 3(i)). The orientation relationship between the needle-like $D0_{24}$-Ni_3Ti phase and the Cu matrix is $[11\bar{2}0]_{D0_{24}\text{-}Ni_3Ti}//[110]_{Cu}$ and $(0001)_{D0_{24}\text{-}Ni_3Ti}//(1\bar{1}\bar{1})_{Cu}$.

It is worth noting that there are different morphologies of $D0_{24}$-Ni_3Ti phases in the alloy, including needle-like, disc-like, and rod-like structures. It was verified by the polar diagram that the orientation relationships between the disc-like phase in Region 5 and the needle-like phase in Region 6 with the Cu matrix are the result of the same orientation relationship observed along different directions. In the case of neglecting the positive and negative signs, $\{111\}_{Cu}$ has four equivalent directions. Therefore, the difference in morphology between the disc-phase and the needle-like phase observed in alloys is attributed to the coherent precipitation of the $D0_{24}$-Ni_3Ti phase in the Cu matrix along various equivalent directions. Meanwhile, the disc-like phase and needle-like phase differ in composition, despite having the same crystal structure as the rod-like phase. The composition of the disc-like phase was measured by TEM−EDS as $Cu_{12.19}Ni_{66.08}Sn_{1.68}Ti_{20.05}$ (at.%), which has a slightly lower Ti content compared to the rod-like $D0_{24}$-Ni_3Ti phase composition ($Cu_{9.03}Ni_{67.96}Sn_{0.12}Ti_{22.90}$ (at.%)) measured by EPMA. In addition, the amount of Cu dissolved in the $D0_{24}$-Ni_3Ti phases is lower compared to those of the $D0_{22}$ and $L1_2$-γ' phases, which have a composition close to Ni_2CuSn [21]. Furthermore, the Cu content decreases as the size increases.

3.3 Variation of hardness and conductivity of alloys with Ti content

After the solid solution treatment at 850 °C for 1 h, the dendrites and discontinuous precipitation of the as-cast alloys are completely dissolved. According to the previous investigation [19], the $Cu_{80}Ni_{15}Sn_5$ alloy reached peak aging at 400 °C for 2 h. The hardness, conductivity, and microstructure evolutions with Ti content x in $Cu_{80}Ni_{15}Sn_{5-x}Ti_x$ (x=0, 0.1875, 0.625, 1.25, 1.875, and 2.5 at.%) alloys aged at 400 °C for 2 and 5 h are displayed in Fig. 4.

In the $Cu_{80}Ni_{15}Sn_5$ reference alloy, the discontinuous precipitation occurs at the grain boundary after aging treatment at 400 °C for 2 h (Fig. 4(a_1)). With the prolonged aging time of 5 h, the volume fraction of discontinuous precipitation increases (Fig. 4(b_1)), resulting in a decrease in hardness and an increase in conductivity. Primarily, the growth of discontinuous precipitated phases continuously consumes the $D0_{22}$-γ' and $L1_2$-γ' phases with main strengthening effect. Therefore, the decrease in hardness is caused by the reduction in the volume fraction of the nano-sized strengthening phases over an extended aging period. Meanwhile, the solutes (Ni and Sn) continuously precipitate from the matrix during aging. As a result, the Cu matrix, serving as the conductive body, is continuously purified, reducing electron scattering and increasing conductivity. The discontinuous precipitation of grain boundaries can greatly damage the mechanical properties of the alloy and lead to cracking of the workpiece during subsequent processing [29].

After adding Ti, the discontinuous precipitation is still completely inhibited even after aging treatment at 400 °C for 5 h, as shown in Figs. 4(b_2−b_6). This demonstrates the superior thermal stability of the alloy compared to the reference alloy. It is beneficial to the subsequent machining process of the alloys.

According to the variations in hardness and conductivity with the Ti content x of $Cu_{80}Ni_{15}Sn_{5-x}Ti_x$ alloys after aging at 400 °C for 2 h and at 400 °C for 5 h, the following phenomena can be observed:

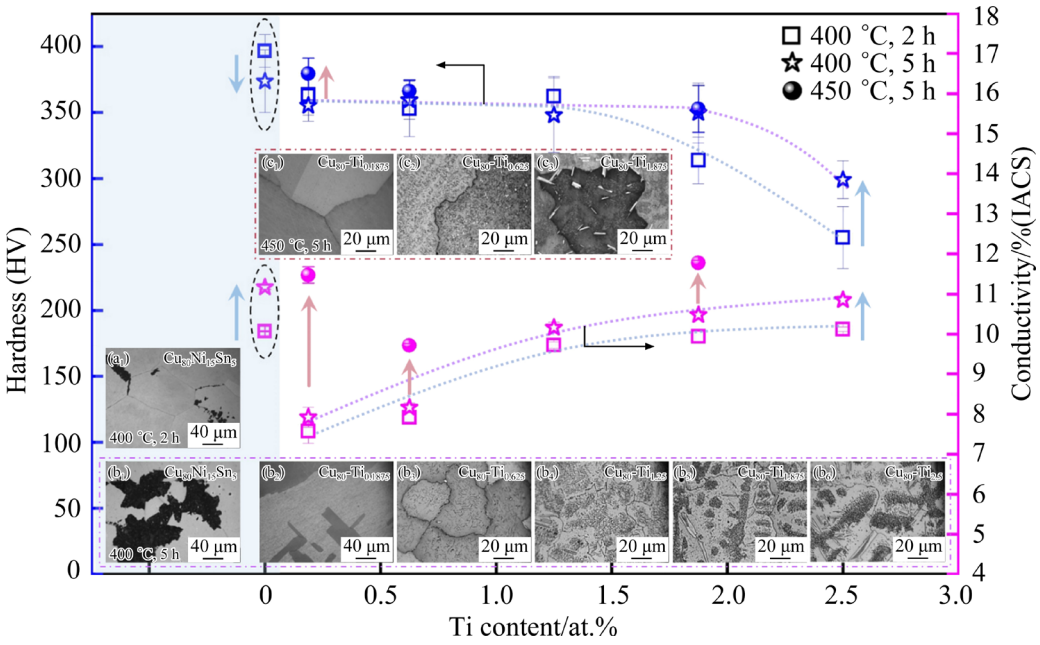

Fig. 4 Hardness and conductivity of $Cu_{80}Ni_{15}Sn_{5-x}Ti_x$ alloys aged at 400 °C for 2 and 5 h or 450 °C for 5 h with Ti content; Microstructures of $Cu_{80}Ni_{15}Sn_{5-x}Ti_x$ alloys aged at 400 °C for 2 h (a_1), 5 h (b_1−b_6) and at 450 °C for 5 h (c_1−c_3)

(1) The hardness and conductivity of the alloys exhibit the same variation trend with x, regardless of the aging time. As x increases, the hardness of the alloy initially remains constant and then decreases, while the conductivity keeps increasing.

(2) For the alloys with a longer aging time of 5 h, the hardness remains constant for a larger range of x and decreases to a less extent. Additionally, the conductivity is higher. This indicates that when the aging time is extended from 2 to 5 h, precipitated phase continues to generate, suggesting that the addition of Ti delays the peak age-hardening process of the alloy and is beneficial to enhancing the thermal stability of the alloy at 400 °C.

The aging temperature was set at 400 °C to promote the precipitation of $D0_{22}$ and $L1_2$-γ' phases and to delay the generation of discontinuous precipitation in the Cu−Ni−Sn alloy. According to studies on Cu−Ni−Ti based alloys [30,31], a temperature range of 450−500 °C is preferred to facilitate the precipitation of Ni−Ti compounds, including the nano-scale $L1_2$-Ni_3Ti phase and the micron-size $D0_{24}$-Ni_3Ti phase. Thus, the aging treatment of 450 °C for 5 h on the $Cu_{80}Ni_{15}Sn_{5-x}Ti_x$ (x=0.1875, 0.625, and 1.875 at.%) alloys was designed to further optimize the properties of the $Cu_{80}Ni_{15}Sn_{5-x}Ti_x$ alloys. The discontinuous precipitation still disappears after increasing the aging temperature (Figs. 4(c_1−c_3)). The hardness and conductivity of the alloys (as indicated by the round ball in Fig. 4) are greatly improved compared to those of the aging treatment at 400 °C for 5 h. Particularly, the Cu_{80}−$Ti_{0.1875}$ alloy exhibits higher hardness and conductivity, reaching HV 379.3 and 11.47%(IACS), respectively.

In summary, Ti plays a role in suppressing discontinuous precipitation at the grain boundary and improving the thermal stability of the alloys. However, it is important to note that excellent properties can only be obtained with the appropriate amount of additives. The aging temperature is increased to 450 °C, which is more conducive to improving the overall performance of the alloys.

4 Discussion

4.1 Evolution of hardness and conductivity

The variation in hardness and conductivity of an alloy is closely related to solid solution and precipitation, which can be simply and directly reflected by the movement of the XRD diffraction peak position.

Figure 5(a) shows the XRD patterns of $Cu_{80}Ni_{15}Sn_{5-x}Ti_x$ (x=0, 0.1875, 0.625, 0.125, 1.875, and 2.5 at.%) alloys after aging at 400 °C for 5 h. In

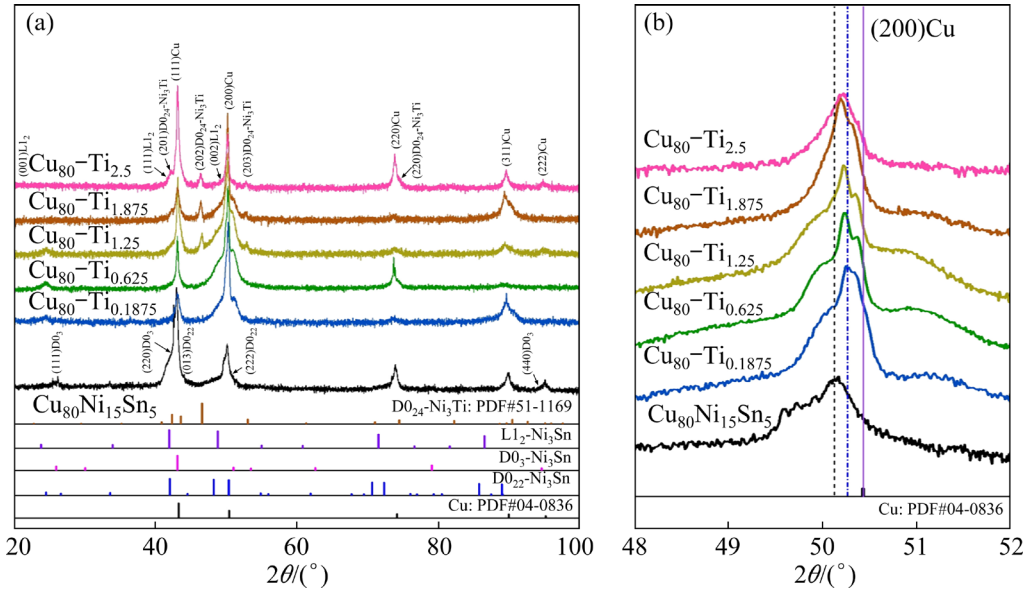

Fig. 5 XRD patterns of $Cu_{80}Ni_{15}Sn_{5-x}Ti_x$ (x=0, 0.1875, 0.625, 1.25, 1.875 and 2.5, at.%) alloys aged at 400 °C for 5 h: (a) Overall patterns; (b) Local magnified patterns

the $Cu_{80}Ni_{15}Sn_5$ alloy, diffraction peaks of the Cu matrix can be observed, along with weak diffraction peaks of the $D0_{22}$ or $L1_2$-γ' phase and the $D0_3$-γ phase (discontinuous precipitation). After adding Ti, the diffraction peaks of the $D0_3$-γ phase disappear. As x increases up to 1.25 at.%, the diffraction peaks of the $D0_{24}$-Ni_3Ti phase are observed distinctly. By further observing the $(200)_{Cu}$ peaks of the $Cu_{80}Ni_{15}Sn_{5-x}Ti_x$ alloys presented in Fig. 5(b), they are all on the left side of those of pure Cu, and with the increase of x, the $(200)_{Cu}$ peak first moves to the right, and then moves to the left when x is higher than 0.1875 at.%.

The variation of the Cu peak position in the alloys can be influenced by the atomic radii of solutes and the interaction between elements. According to the atomic radii of Cu, Ni, Sn, and Ti, which are 0.128, 0.125, 0.158, and 0.145 nm, respectively, the dissolution of Sn and Ti in the Cu matrix leads to a lattice expansion, while Ni leads to a shrinkage. Therefore, the position of the $(200)_{Cu}$ peak in $Cu_{80}Ni_{15}Sn_{5-x}Ti_x$ alloys is on the left side of pure Cu. In the Cu_{80}−$Ti_{0.1875}$ alloy, the $(200)_{Cu}$ peak is located at the right of the reference alloy, indicating that the Sn and Ti contents in the Cu matrix are lower. This suggests that the volume fraction of the precipitated phases increases. The calculation of the volume fraction of the precipitated phase in the reference alloy and Cu_{80}−$Ti_{0.1875}$ alloy (Fig. 6(a)) using Thermo-calc software yields identical results. When x is higher than 0.1875 at.%, Ti starts to form $L1_2$-Ni_3Ti and $D0_{24}$-Ni_3Ti phases. Compared with $D0_{22}$ and $L1_2$-γ' phases with compositions close to Ni_2CuSn, the precipitation of the Ni_3Ti phase consumes more Ni but less Sn from the Cu matrix. Additionally, the larger the size of the Ni_3Ti phase is, the more the Ni is consumed. Therefore, as x increases, the position of the $(200)_{Cu}$ peak shifts to the left due to the larger lattice parameters of the Cu matrix.

When x is 0.1875 at.%, the alloy is composed of Cu matrix, $D0_{22}$, and $L1_2$-γ' phases, which is consistent with the reference alloy presented in Figs. 6(b−d). But according to the above results, the volume fraction of $D0_{22}$ and $L1_2$-γ' phases increases, but the hardness decreases slightly compared to that of the reference alloy, which is due to a slight increase in the size of $D0_{22}$ and $L1_2$-γ' phases, which weakens the strengthening effect after the addition of Ti. As x continues to increase, the hardness remains relatively constant and then decreases. This indicates that there is a balance between the increase in precipitation amount and the growth of the precipitated phase, until the generation of abundant micron-sized $D0_{24}$-Ni_3Ti phases with a weaker strengthening effect.

Previous study [21] has clarified that the conductive body of the Cu−Ni−Sn alloy is the Cu matrix, so the conductivity of the alloy is mainly related to the content of solutes in the Cu matrix.

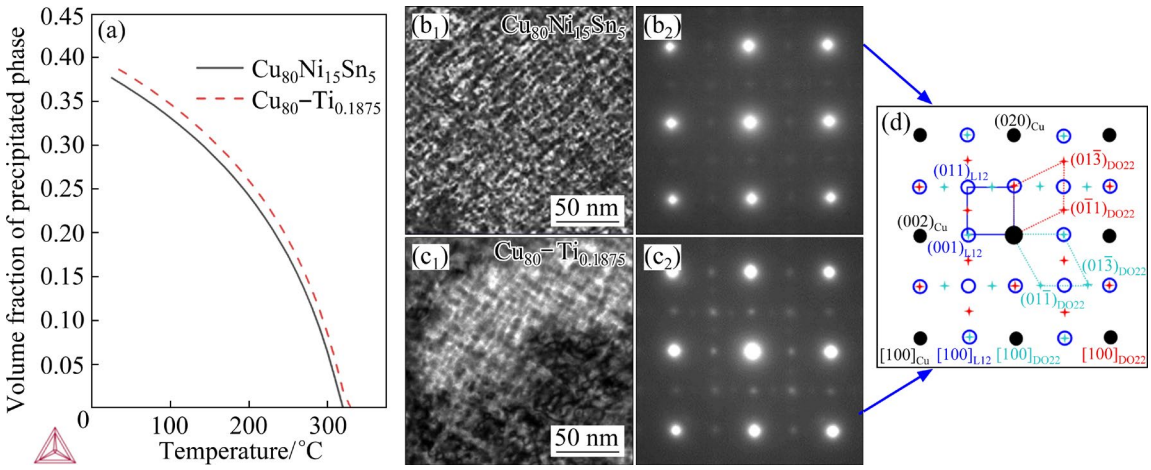

Fig. 6 Volume fractions of precipitated phases in $Cu_{80}Ni_{15}Sn_{5-x}Ti_x$ (x=0 and 0.1875, at.%) alloys calculated by Thermo-calc software (a), bright field TEM images and corresponding SAED patterns of $Cu_{80}Ni_{15}Sn_{5-x}Ti_x$ (x=0, 0.1875 at.%) alloys aged at 400 °C for 5 h (b_1, b_2, c_1, c_2), and their calibration schematic diagram (d)

The effect of a single solute element on the resistivity of pure Cu has been thoroughly examined. It has been revealed that the resistivity increase due to the dissolution of 1 at.% Ni, 1 at.% Sn and 1 at.% Ti is 1.111×10^{-8}, 3.056×10^{-8} and 16.364×10^{-8} Ω·m, respectively [32]. Obviously, the effect of dissolved Ti on resistivity of the Cu matrix is much greater than that of Ni and Sn. But fortunately, Ti has a favorable role in promoting precipitation, so the conductivity of Ti-containing alloy is slightly lower compared with that of the reference alloy. In addition, with the increase of x, the precipitation of solutes also increases, leading to a corresponding increase in conductivity.

4.2 Inhibition mechanism of discontinuous precipitation

The discontinuous precipitation preferentially nucleates at grain boundaries and grows towards the grain by depleting the $D0_{22}$ or $L1_2$-γ' phases [33]. It is premised on the segregation of Sn to grain boundaries, and is thus essentially a problem of destabilization and diffusion of the matrix and precipitated phases. In the Cu−Ni−Sn−Ti alloy, Ti is partially dissolved in both the Cu matrix and the $D0_{22}$ and $L1_2$-γ' phases. The strong enthalpic interaction between Ti and Cu, Ni, or Sn can retard the long-range diffusion of Sn during aging and enhance the stability of the alloy, thereby suppressing the generation of discontinuous precipitation. Currently, the above results of this work have verified that the discontinuous precipitation is effectively inhibited by the addition of Ti to the Cu−Ni−Sn alloy.

According to the previous study, the growth rate of discontinuous precipitation (G) can be given by the following formula [34]:

$$G=MP \tag{1}$$

where M represents the mobility of the boundary and P represents the driving force for the growth. The P consists of four parts: the driving force due to the solute concentration difference (P_C), the driving force due to the strain energy difference (P_S), the driving force due to interfacial energy difference between the matrix and the discontinuous precipitation (P_I), and the resistance force to the advancing boundary migration caused by precipitated phases in the matrix (P_P).

In this work, Ti was added by replacing Sn, which is the primary constituent element of the discontinuous precipitated phase. With other parameters remaining constant, a decrease in Sn content reduces the driving force component of compositional variation, thereby decreasing the growth driving force (P_C) for discontinuous precipitation. In addition, it has been reported that the insoluble particles separated at the grain boundary contribute to the suppression of discontinuous precipitation [18]. The $D0_{24}$-Ni_3Ti phases located at the grain boundary not only occupy the nucleation sites of discontinuous precipitation in Cu−Ni−Sn−Ti alloys, such as Cu_{80}−$Ti_{0.625}$ and Cu_{80}−$Ti_{1.875}$ alloys presented in

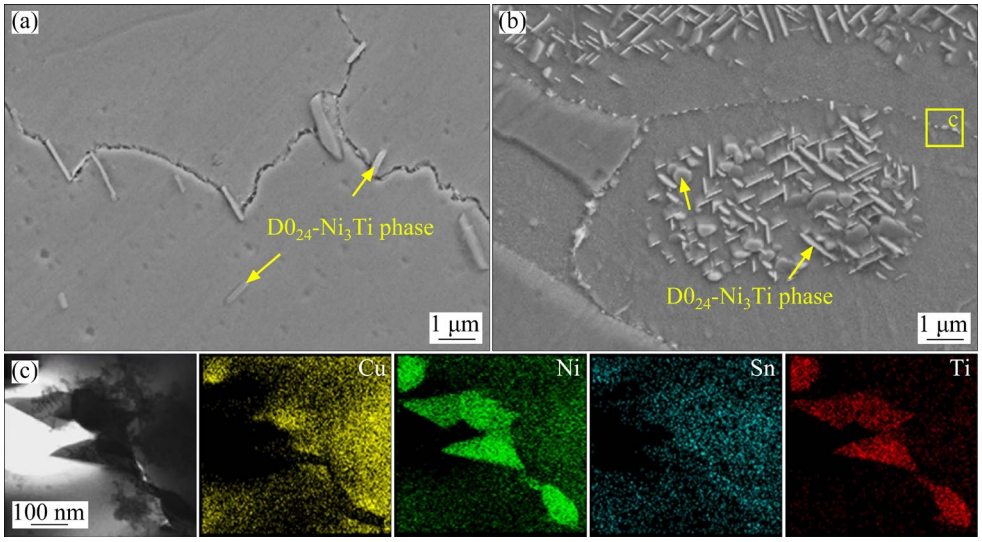

Fig. 7 SEM images of $Cu_{80}Ni_{15}Sn_{5-x}Ti_x$ (x=0.625 and 1.875, at.%) alloys aged at 400 °C for 5 h, respectively (a, b), and BF image and in-situ EDS single element mappings of precipitated phases at grain boundary (c)

Figs. 7(a−c), but also have a pinning effect on the grain boundary, hindering the motion of the grain boundary and reducing the mobility (M) of the advancing boundary. More importantly, the $D0_{24}$-Ni_3Ti phases precipitated within the grain (Fig. 7(b)) greatly increase the resistance force (P_P) to the migration of the boundary during advancement. Therefore, the addition of Ti to the Cu−Ni−Sn alloy is beneficial to suppressing the nucleation and growth of discontinuous precipitate phases in the alloy.

4.3 Evaluation of comprehensive properties of alloys

The comprehensive performance of $Cu_{80}Ni_{15}Sn_{5-x}Ti_x$ (x=0, 0.1875, 0.625, 0.125, 1.875, and 2.5 at.%) alloys is evaluated by hardness and electrical resistivity, as displayed in Fig. 8. In order to clearly demonstrate the performance advantages of $Cu_{80}Ni_{15}Sn_{5-x}Ti_x$ alloys, $Cu_{80}Ni_{15}Sn_{4.375}M_{0.625}$ (M=Si, Zn, or Co) [19,28], Cu−Be, and Cu−Ni−Sn commercial alloys (C17200 (Cu−2Be (wt.%)) and C72900 (Cu−15Ni−8Sn (wt.%)) are chosen as references. The data for commercial alloys is sourced from the ASM Metals Handbook and Industrial Product Manuals [32,35]. The commercial alloys are consistent with the alloys designed in this work. The dashed lines in Fig. 8 join the data points of the different alloys to the data of pure copper (hardness of HV 88 and resistivity of 1.74 Ω·cm) [32], the slope of which represents the improvement of performance by alloying. The higher the slope is, the better the hardness and conductivity of alloys are, which is located in upper left area in Fig. 8.

Currently, C17200 (Cu−2Be (wt.%)) alloy has the best comprehensive performance due to the highest slope of corresponding dashed line in Fig. 8. However, Be is a toxic element and there is emitting of toxic gases during processing of Cu−Be alloys, which is a disadvantage for the ecological environment. The C72900 (Cu−15Ni−8Sn (wt.%)) alloy has a lower slope, which is the reason why the overall properties of the Cu−Ni−Sn series alloys need to be improved. Evidently, the increase in the

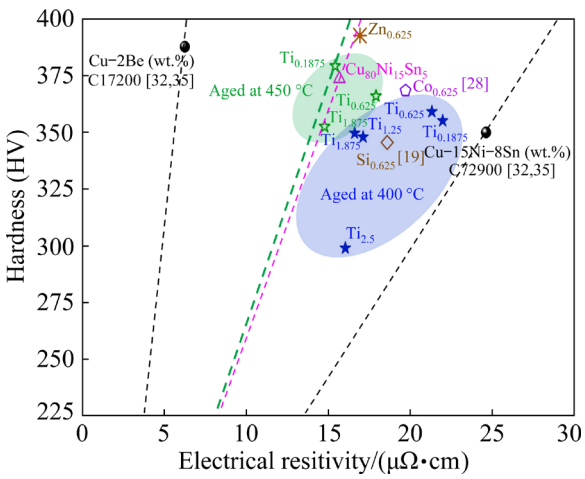

Fig. 8 Relationship between electrical resistivity and hardness in C17200 (Cu−2Be), C72900 (Cu−15Ni−8Sn) commercial alloys [32,35], Cu−Ni−Sn−Si (Zn or Co) [19,28], and Cu−Ni−Sn−Ti alloys aged at 400 and 450 °C in this work

slope of the dashed line indicates that alloying can lead to a significant improvement in the overall performance improvement of Cu−Ni−Sn alloys. Among them, Ti-containing alloys all have lower electrical resistivity than the C72900 alloy, as well as higher hardness, except for the Cu_{80}−$Ti_{2.5}$ alloy aged at 400 °C for 5 h. The addition of Ti can effectively inhibit the Sn segregation and discontinuous precipitation in both the C72900 alloy and the $Cu_{80}Ni_{15}Sn_5$ alloy, as designed by the cluster-plus-glue-atom model in this work. When the aging temperature increases from 400 to 450 °C, the overall properties of Ti-containing alloys are improved. Compared to other added elements such as Si, Zn, or Co, the enhancement effect brought by Ti is superior.

5 Conclusions

(1) The addition of Ti to $Cu_{80}Ni_{15}Sn_5$ alloy can significantly suppress the discontinuous precipitation, promote the precipitation of solutes in the Cu matrix, and improve the high-temperature stability of the alloy.

(2) When the Ti content is 0.1875 at.%, Ti is mainly solid soluble in the Cu matrix, $D0_{22}$ and $L1_2$-γ' phases. With the increase of Ti content, $L1_2$-Ni_3Ti phase which is coherent with the matrix and $D0_{24}$-Ni_3Ti phase which has a certain orientation relationship with the matrix can be introduced.

(3) With the increase of Ti content, the hardness of the alloy initially remains essentially constant and then decreases, while the conductivity keeps increasing.

(4) Compared to aging at 400 °C, 450 °C is more favorable for alloy properties, especially the Cu_{80}−$Ti_{0.1875}$ alloy after aging at 450 °C for 5 h, the hardness and conductivity exceed those of $Cu_{80}Ni_{15}Sn_5$ alloy. Compared to other added elements such as Si, Zn, or Co, Ti has a greater impact on enhancing the overall performance. Therefore, Ti can be adopted as an effective additive element for the Cu−Ni−Sn alloy system, but the amount of addition needs to be controlled.

CRediT authorship contribution statement

Ying-lin HU: Writing − Original draft, Data curation, Investigation, Formal analysis; **Zi-luo CHENG:** Writing − Review & editing, Investigation; **Xiao-na LI:** Conceptualization, Methodology, Formal analysis, Supervision; **Zhu-min LI:** Writing − Review & editing; **Yuan-di HOU** and **Min LI:** Investigation, Formal analysis; **Mian YANG:** Data curation; **Yue-hong ZHENG:** Writing − Review & editing; **Chuang DONG:** Conceptualization, Supervision.

Declaration of competing interest

The authors declare that they have no known competing financial interests or personal relationships that could have appeared to influence the work reported in this paper.

Acknowledgments

We would like to gratefully acknowledge the financial support from the National Natural Science Foundation of China (No. 52071052).

References

[1] LUO Bao-min, LI Dao-xi, ZHAO Chao, WANG Zhi, LUO Zong-qiang, ZHANG Wei-wen. A low Sn content Cu−Ni−Sn alloy with high strength and good ductility [J]. Materials Science and Engineering A, 2019, 746: 154−161.

[2] ZHANG Yang, XIAO Zhu, ZHAO Yu-yuan, LI Zhou, XING Ying, ZHOU Ke-chao. Effect of thermo-mechanical treatments on corrosion behavior of Cu−15Ni−8Sn alloy in 3.5 wt.% NaCl solution [J]. Materials Chemistry and Physics, 2017, 199: 54−66.

[3] SINGH J B, CAI W, BELLON P. Dry sliding of Cu−15wt.%Ni−8wt.%Sn bronze: Wear behaviour and micro-structures [J]. Wear, 2007, 263(1): 830−841.

[4] GUO Cheng-jun, CHEN Jin-shui, WANG Hang, XIAO Xiang-peng, HUANG Hao, YANG Bin. Effect of P addition on dry sliding wear properties of Cu−15Ni−8Sn alloy [J]. The Chinese Journal of Nonferrous Metals, 2021, 31(5): 1156−1167. (in Chinese)

[5] CRIBB W R, GRENSING F C. Spinodal copper alloy C72900−new high strength antifriction alloy system [J]. Canadian Metallurgical Quarterly, 2011, 50(3): 232−239.

[6] ZHANG Wei-wei, ZHAO Zhi-he, FANG Ji-hua, HE Ping, CHAO Zhen-long, GONG Deng, CHEN Guo-qing, JIANG Long-tao. Evolution and strengthening mechanism of metastable precipitates in Cu−2.0wt.%Be alloy [J]. Journal of Alloys and Compounds, 2021, 857: 157601.

[7] JIANG Yan-bin, ZHANG Tong-tong, LEI Yu, HE Shuang-jiang, LIU Xin-hua, XIE Jian-xin. Effects of Ni content on microstructure and properties of aged Cu−0.4Be alloy [J]. Transactions of Nonferrous Metals Society of China, 2021, 31(3): 679−691.

[8] ZHAO J C, NOTIS M R. Spinodal decomposition, ordering transformation, and discontinuous precipitation in a Cu−15Ni−8Sn alloy [J]. Acta Materialia, 1998, 46(12): 4203−4218.

[9] ZHAO J C, NOTIS M R. Microstructure and precipitation kinetics in a Cu−7.5Ni−5Sn alloy [J]. Scripta Materialia,

1998, 39(11): 1509−1516.

[10] ZHAO Chao, WANG Zhi, LI Dao-xi, KOLLO L, LUO Zong-qiang, ZHANG Wei-wen, PRASHANTH K G. Selective laser melting of Cu−Ni−Sn: A comprehensive study on the microstructure, mechanical properties, and deformation behavior [J]. International Journal of Plasticity, 2021, 138: 102926.

[11] WANG J B, ZHOU X L, LI J H, BROCHU M, ZHAO Y F. Microstructures and properties of SLM-manufactured Cu−15Ni−8Sn alloy [J]. Additive Manufacturing, 2020, 31: 100921.

[12] HERMANN P, MORRIS D G. Relationship between microstructure and mechanical properties of a spinodally decomposing Cu−15Ni−8Sn alloy prepared by spray deposition [J]. Metallurgical and Materials Transactions A, 1994, 25: 1403−1412.

[13] LI Ji-kang, ZHANG Jing-kai, ZHANG Zhen-wu, LI Wei, WEI Qing-song. Microstructure, tensile and tribological properties of Cu−15Ni−8Sn alloy fabricated by selective laser melting [J]. The Chinese Journal of Nonferrous Metals, 2023, 33(2): 386−399. (in Chinese)

[14] WANG Nan, SHEN Yi-di, AN Qi, REDDY K M, JIN Ming-jiang, KARRE R, WANG Xiao-dong. Microstructure evolution and mechanical property of Cu−15Ni−8Sn−0.2Nb alloy during aging treatment [J]. Journal of Materials Science & Technology, 2021, 86: 227−236.

[15] GUO Cheng-jun, CHEN Jin-shui, XIAO Xiang-peng, HUANG Hao, WANG Wen-jing, YANG Bin. The effect of Co addition on the modulated structure coarsening and discontinuous precipitation growth kinetics of Cu−15Ni−8Sn alloy [J]. Journal of Alloys and Compounds, 2020, 835: 155275.

[16] GUO Cheng-jun, WAN Jia, CHEN Jin-shui, XIAO Xiang-peng, HUANG Hao, LIU Jing-ping, YANG Bin. Inhibition of discontinuous precipitation and enhanced properties of Cu−15Ni−8Sn alloy with Fe addition [J]. Materials Science and Engineering A, 2020, 795: 139917.

[17] GUO Zhong-kai, JIE Jin-chuan, LIU Shi-chao, ZHANG Yu-bo, QIN Bai-liang, WANG Tong-min, LI Ting-ju. Effect of V addition on microstructures and mechanical properties of Cu−15Ni−8Sn alloy [J]. Materials Science and Engineering A, 2019, 748: 85−94.

[18] OUYANG Yi, GAN Xue-ping, ZHANG Shi-zhong, LI Zhou, ZHOU Ke-chao, JIANG Ye-xin, ZHANG Xian-wei. Age-hardening behavior and microstructure of Cu−15Ni−8Sn−0.3Nb alloy prepared by powder metallurgy and hot extrusion [J]. Transactions of Nonferrous Metals Society of China, 2017, 27(9): 1947−1955.

[19] YU Q X, LI X N, WEI K R, LI Z M, ZHENG Y H, LI N J, CHENG X T, WANG C Y, WANG Q, DONG C. Cu−Ni−Sn−Si alloys designed by cluster-plus-glue-atom model [J]. Materials & Design, 2019, 167: 107641.

[20] GUO Zhong-kai, JIE Jin-chuan, LIU Shi-chao, LIU Jia-ming, YUE Shi-peng, ZHANG Yu-bo, LI Ting-ju. Suppression of discontinuous precipitation in age-hardening Cu−15Ni−8Sn alloy by addition of V [J]. Journal of Alloys and Compounds, 2020, 813: 152229.

[21] YANG M, HU Y L, LI X N, LI Z M, ZHENG Y H, LI N J, DONG C. Compositional interpretation of high elasticity Cu−Ni−Sn alloys using cluster-plus-glue-atom model [J]. Journal of Materials Research and Technology, 2022, 17: 1246−1258.

[22] TAKEUCHI A, INOUE A. Classification of bulk metallic glasses by atomic size difference, heat of mixing and period of constituent elements and its application to characterization of the main alloying element [J]. Materials Transactions, 2005, 46(12): 2817−2829.

[23] WEI Huan, CUI Yan-chao, CUI Hui-qi, WEI Ying-hui, HOU Li-feng. Effects of multiple trace alloying elements on the microstructure and properties of Cu−4wt.%Ti alloys [J]. Materials Science and Engineering A, 2017, 707: 392−398.

[24] HEO Y U, TAKEGUCHI M, FURUYA K, LEE H C. Transformation of DO24 η-Ni_3Ti phase to face-centered cubic austenite during isothermal aging of an Fe−Ni−Ti alloy [J]. Acta Materialia, 2009, 57(4): 1176−1187.

[25] SHANKAR K V, PAUL C, SELLAMUTHU R. Development of Cu−6Sn−5Ni−xTi and to analyse their mechanical and wear properties in as-cast condition [J]. International Journal of Microstructure and Materials Properties, 2017, 12: 94−103.

[26] ZHAO Chao, ZHANG Wei-wen, WANG Zhi, LI Dao-xi, LUO Zong-qiang, YANG Chao, ZHANG Da-tong. Improving the mechanical properties of Cu−15Ni−8Sn alloys by addition of titanium [J]. Materials (Basel, Switzerland), 2017, 10(9): E1038.

[27] MIKI M, OGINO Y. Effects of doped elements on the cellular precipitation in Cu−10Ni−8Sn alloy [J]. Materials Transactions, JIM, 1994, 35(5): 313−318.

[28] LI N J, LI X N, LI Z M, YU Q X, ZHENG Y H, HU Y L, WANG Q, DONG C, JIANG Y X, ZHANG X W. Differential effects of Zn and Co solutes on the properties of Cu−Ni−Sn alloys [J]. Intermetallics, 2020, 125: 106894.

[29] CARIS J, LI D Q, STEPHENS J J, LEWANDOWSKI J J. Microstructural effects on tension behavior of Cu−15Ni−8Sn sheet [J]. Materials Science and Engineering A, 2010, 527(3): 769−781.

[30] KNIGHTS R, WILKES P. The precipitation of titanium in copper and copper−nickel base alloys [J]. Acta Metallurgica, 1973, 21(11): 1503−1514.

[31] LIU Qing, WANG Tong-he, JIAO Jun, WANG Wei, LIU Huan-yu, ZHANG Xiao, ZHANG Chao-xian, QI Fu-gong, JIE Jin-chuan, XU Xue-xia, DING Hai-min. The microstructures and properties of diamond reinforced Cu−Ni−Si−Ti alloys [J]. Materials Science and Engineering A, 2023, 862: 144478.

[32] DAVIS J. ASM specialty handbook: Copper and copper alloys [M]. New York: ASM International, 2001.

[33] GUO Cheng-jun, SHI Yu-fan, XIAO Xiang-peng, YOU Shu-ming, AN Gui-huan, GONG Ya-hui, YANG Bin. Enhanced softening resistance and mechanical properties of Cu−Ni−Sn alloy with Al, Zn and Si micro-alloying [J]. Journal of Alloys and Compounds, 2022, 923: 166410.

[34] MIKI M, OGINO Y. Effect of Si addition on the cellular precipitation in a Cu−10Ni−8Sn alloy [J]. Materials Transactions, JIM, 1990, 31(11): 968−974.

[35] JOSEPH G, KUNDIG K J A. Copper: Its trade, manufacture, use, and environmental status [M]. New York: ASM International, 1998.

添加微量 Ti 调控 Cu−Ni−Sn 合金的显微组织与性能

胡莹琳[1]，程子洛[1]，李晓娜[1,2]，利助民[3]，侯远迪[1]，李 敏[1]，杨 冕[1]，郑月红[4]，董 闯[1,2]

1. 大连理工大学 材料科学与工程学院，大连 116024；
2. 大连理工大学 三束材料改性教育部重点实验室，大连 116024；
3. 安徽工程大学 材料科学与工程学院，芜湖 241000；
4. 兰州理工大学 省部共建有色金属先进加工与再利用国家重点实验室，兰州 730050

摘 要：Sn 偏析和晶界处不连续析出会恶化 Cu−Ni−Sn 合金的强度、塑性和可加工性。为了解决上述问题，可通过引入强焓相互作用元素对合金进行多组元化成分设计。本文采用团簇加连接原子模型设计一系列 $Cu_{80}Ni_{15}Sn_{5-x}Ti_x$(摩尔分数，%)合金，然后利用 TEM 等分析方法系统研究了 Ti 含量对合金显微组织及性能的影响。结果表明，Ti 能有效抑制偏析和不连续析出，同时促进连续析出，从而提高合金的高温稳定性。随着 Ti 含量的增加，Ti 在合金中的分布方式从均匀分布转变为以析出为主。当 Ti 处于固溶状态时，合金的硬度和电导率均超过 C72900 (Cu−15Ni−8Sn (质量分数，%))工业合金和 $Cu_{80}Ni_{15}Sn_5$ (摩尔分数，%)参比合金。

关键词：Cu−Ni−Sn 合金；显微组织；性能；团簇加连接原子模型；偏析；不连续析出；焓相互作用

(Edited by Wei-ping CHEN)